10 Chemical processes in intense optical fields

Brian Sheehy

National Synchrotron Light Source, Brookhaven National Laboratory, Upton, New York, 11973, USA

1 Introduction

The electromagnetic fields attainable by most laboratory sources are miniscule compared with the fields that bind atoms and molecules and define their chemical properties. Consequently, probing atoms and molecules with these sources has been a matter of investigating small perturbations on a pre-defined system, and the chemical manipulation of matter has historically been confined to the subtle exploitation of the atomic and molecular structures already provided by nature, without the possibility of shaping the dynamics and redefining the fundamental structures themselves. In the last decade, improvements in laser technology have provided optical fields whose strength approaches and exceeds atomic and molecular binding fields, and the means of precisely controlling the time, amplitude, and phase characteristics of these fields. In addition to posing a challenging new set of physical questions, these developments make it possible for the first time to consider controlling reactions by manipulating atomic and molecular structure itself, and controlling the evolution of quantum mechanical systems on molecular time scales.

From the point of view of fundamental interactions, an entirely new regime of dynamics has been opened to investigation. A host of new nonlinear phenomena have been observed, and the theory has evolved new techniques for handling the difficult numerical calculations, as well as new paradigms for understanding the essential physics. In some of these models, a great deal of the physics can be understood in terms of relatively simple pictures. In this review, we will discuss the growth in the understanding of the fundamental interactions as they apply first to atoms, and then to molecules in the gas phase. We will then discuss some of the progress that has been made in exploiting this understanding to manipulate and control molecular systems at the quantum level.

An atom in a strong field may in general absorb a large number of photons—many more than are required to reach the ionization threshold of the atom. This above-threshold ionization (ATI) was first observed in 1979 by Agostini *et al*,[1] manifesting itself in the energy spectrum of the photoelectrons as a series of peaks separated by the photon energy. These electrons can be extremely energetic: electron energies approaching a kilovolt have been produced by an optical field in which the photon energy was only 1.6 eV.[2] ATI is just one possibility; the absorbed photons can also be

converted to a single energetic photon, a process known as high harmonic generation (HHG).[3] This process is a promising source of both extremely short-wavelength and short-pulsewidth radiation: harmonic orders of several hundred have been produced, to wavelengths less than 3 nm,[4] and there is good reason to believe that HHG may be used to form subfemtosecond pulses.[5–8]

A third possibility is the removal of multiple electrons, either sequentially or nonsequentially. The possibility of nonsequential, correlated multiple emission motivated a number of early strong field studies (see ref. 9 for a discussion), but early experiments indicating correlated emission were later shown to be attributable to higher order sequential processes. More recently, experiments in the rare gases have demonstrated nonsequential multiple ionization.[2,10–12] The nature of this process, and in particular, the role that electron correlation plays in it, is still rather controversial, and is discussed further below.

A simple picture connecting all three processes, ATI, HHG, and nonsequential ionization, has been developed.[13–15] In sufficiently intense optical fields, the instantaneous Stark potential seen by a valence electron presents a barrier through which the electron may tunnel into the continuum. Once in the continuum, the electron's motion in the oscillating optical field is quite simple. It may return to the ion core, after acquiring energy from the optical field, and interact. The three possible interactions, elastic scattering, recombination, and inelastic scattering, may be related to ATI, HHG, and nonsequential ionization respectively. We will explore this picture and its limitations in section 2.

This simple picture of ionization plus interaction has an interesting analog in molecular photodissociation. In 1987, Frasinski *et al.*[16] suggested that an intense optical field could rapidly strip electrons from a molecule by field ionization while its constituent atoms were at or near their equilibrium configuration. The mutual Coulomb repulsion of the ionized fragments left behind might then account for the large kinetic energies of the photofragments observed in strong field photodissociation experiments. What is more, the momenta of these photofragments could be used to reconstruct the molecule's equilibrium configuration. The dynamics of such 'Coulomb explosions' have turned out to be more subtle: ionization may be correlated with nuclear motion, and the precise mechanism is still controversial. These topics will be discussed in section 4, following a more general discussion of strong field dissociation in section 3.

Several avenues have been taken in exploiting strong field interactions for chemical control. It is useful to think of approaching the problem in the time domain or the frequency domain. In the time-domain approach, first introduced by Tannor and Rice,[17] an initial optical interaction is used to create a wave packet—a carefully phased superposition of eigenstates of the system under study. The relative phases in the superposition are controlled through the amplitudes and phases of the spectral components of the light that creates the wave packet. The wave packet evolves, and at some optimal later time, another optical interaction drives the system towards the desired output state. Examples of this technique have been experimentally demonstrated in the photodissociation of NaI, by Zewail and coworkers,[18] and in the photoionization of Na_2 by Baumert and Gerber.[19]

This picture suggests that detailed knowledge of the dynamics of the system under study, as well as a considerable degree of finesse, is required for control. Planning the

motion of wave packets along incompletely known potential surfaces sounds difficult. In reality, it is not necessary to understand everything that is happening in a reaction in order to optimize a particular outcome. An equally effective approach is to vary the free parameters of the optical field that interacts with the system in response to a feedback signal related to the presence of the desired output. The problem then becomes one of developing a learning algorithm that directs the variations of the optical field towards a converged optimal solution. This 'optimal control', first introduced by Rabitz and coworkers,[20] has been demonstrated experimentally in a number of different systems.[21–24] This very general technique promises to become a versatile tool even beyond control applications: from analyzing intramolecular forces to quantum computing.[25]

Approaching the problem in the frequency domain, one can think of manipulating reactions by coupling initial and final states by multiple pathways with well-defined relative phases. This is analogous to Young's two-slit experiment: instead of a relative phase between two paths taken by a plane wave being varied by the geometry of source and slits, the relative phase between multiple couplings of initial to final state is varied through an interaction. By varying the phase between the couplings, the outcome of the reaction can be controlled. This "coherent control" was introduced by Brumer and Shapiro,[26] who proposed that the multiple paths could be created by two different lasers that coupled the initial and final states by different numbers of photons. Using nonlinear optical generation techniques, it is possible to generate such multiple frequencies with a well-defined and controllable relative optical phase. The phase between the couplings is then determined by this optical phase, and the photon orders of the two couplings, and so the reaction, can be directly manipulated through the optical phase. This technique has been implemented to control photoionization[27–34] and photodissociation[35–38] processes in atoms and molecules, as well as to control photocurrents in semiconductor systems,[39,40] and will be discussed in more detail in section 6.

2 Atomic dynamics

In the simple picture mentioned above, the initial ionization step proceeds by tunneling through the barrier in the potential formed by the atomic and optical fields. Of course, the shape of this barrier is changing periodically at the optical frequency, and the tunneling approximation is only valid in the limit that tunneling occurs faster than the shape of the barrier changes, *i.e.* that the tunneling rate near the peak of the optical field is larger than the optical frequency. At lower intensities, multiphoton couplings (resonant and non-resonant) contribute more to the ionization rate than tunneling. The boundary between the tunneling and multiphoton regimes is parameterized by the dimensionless Keldysh nonadiabaticity parameter γ,[41] which is given by

$$\gamma = \frac{\omega_{\mathrm{L}}}{\omega_{\mathrm{tun}}} = \sqrt{\frac{E_0}{2U_{\mathrm{p}}}},$$

where ω_{L} is the angular frequency of the optical field, ω_{tun} is the tunneling rate at the peak of the optical field, E_0 is the field-free binding energy of the electron, and U_{p} is

the ponderomotive potential. The ponderomotive potential is simply the time-averaged kinetic energy of a free electron oscillating in the optical field, and is given in atomic units by $U_p = 2\pi\alpha I/\omega_L^2$, where α is the fine structure constant. The tunneling approximation improves then, as the value of γ becomes smaller. The boundary between the tunneling and multiphoton regimes is generally taken to be $\gamma \approx 1$.

The transition between the tunneling and multiphoton regimes can be seen in the photoionization yield curve shown in Fig. 1, taken from ref. 2. The intensity dependence of the photoionization of He to form He^+ is compared to two different calculations (the He^{2+} yield curve is discussed below). The solid line, showing the TDSE-SAE calculation, reproduces the data over 12 orders of magnitude in signal. This is a time-dependent calculation in which a difference equation approximation to the Schrödinger equation is solved numerically on a spatial grid, in the single active electron (SAE) approximation.[42] The SAE approximation considers the optical field's interaction with only one electron, which moves in the combined field of the nucleus and the remaining electrons, the latter being frozen in their ground state orbitals. The second calculation (long dashed line) considers only the ionization that occurs through tunneling, and is based upon the work of Ammosov, Delone, and Krainov (ADK).[43]

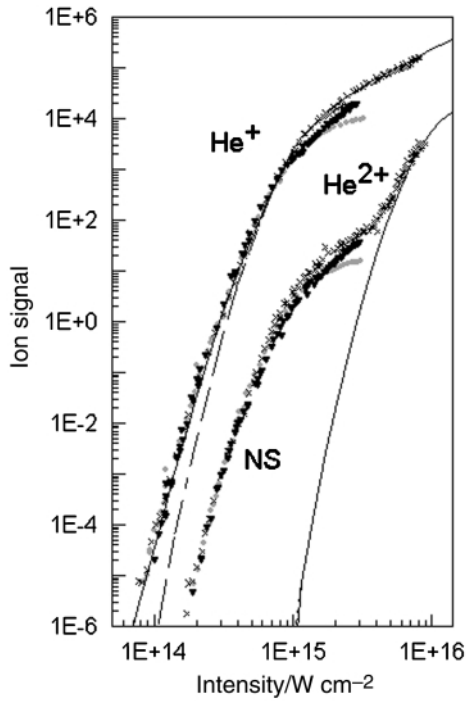

Fig. 1 Measured yields of single and double ionization of helium in a 780 nm, 160 fs (FWHM), linearly polarized laser pulse. The solid lines are TDSE-SAE calculations, while the long dashed line represents the single ionization yield due to tunneling only. In He^{2+}, the nonsequential (NS) rate below the knee is orders of magnitude larger than the predicted sequential rate. Reproduced with permission from ref. 2.

At low intensities, multiphoton processes are relatively more important, and the ADK rate underestimates the yield considerably. Above 5×10^{14} W cm^{-2}, which in the experimental conditions corresponds to a value of $\gamma = 0.7$, the ADK rate is a very good approximation.

When tunneling is the dominant mechanism, much of the essential physics of strong field optical–atomic interactions can be explained in terms of 'rescattering'—the interaction of the ion core with an electron which has tunneled into the continuum and is subsequently returned to the core by the optical field.[13] The first success of the rescattering model was in predicting the cutoff in the high-energy photon yield observed in high harmonic generation.[14,15] In a typical HHG spectrum, produced by focusing short-pulse near-infrared radiation in a rare gas jet, the lowest order harmonics are produced in the largest volume, at the lowest intensity parts of the focus, and their yield falls off quickly with increasing harmonic order. A strongly nonperturbative plateau in the yield curve extends from this low-order fall off to a sudden cutoff at very high photon energy. The intensity at which this high-energy cutoff occurs is intensity-dependent, moving to higher energy in proportion to the peak optical intensity. If the harmonic energy is measured in units of the ponderomotive potential U_p, which, as noted above, is also linear in the optical intensity, the overall shape of the curve does not change with intensity, and the high-energy cutoff falls at $3.2U_p + I_p$, where I_p is the ionization potential of the neutral atom. This scaling with the ponderomotive potential simply reflects the scaling of the classical motion of the electron in the optical field. An electron tunnels into the continuum with zero kinetic energy, and the energy it acquires from the optical field is a function of the optical phase at which it tunnels, but for all phases is proportional to the field intensity. It is simple to show[14,15] that, if it returns to the core within an optical cycle, the maximum energy it can acquire at that return is $3.2U_p$. If the electron and ion then recombine radiatively, the maximum available energy for the photon is $3.2U_p + I_p$, in agreement with the observed cutoff.

The rescattering model accounts well for many features of photoelectron energy spectra (PES) produced in short-pulse experiments as well. In such experiments, a sample of neutral atoms is subjected to a laser pulse that is sufficiently short that electrons released by ionization do not move over a significant fraction of the focal volume during the time that the pulse is on. This prevents changes to the electron energy due to ponderomotive forces—forces due to the optical intensity gradient in the focus. If the ionization proceeded solely by tunneling, and there was no further interaction of the electron with the ion, then the electron energy that one would expect at the detector is just the drift energy E_{drift} of the electron in the optical field. This is easily obtained by integrating the classical equation of motion, and averaging over an optical cycle:

$$\begin{aligned} m\frac{d\boldsymbol{v}}{dt} &= -e\boldsymbol{E}\sin(\omega t - \varphi) \\ \boldsymbol{v} &= \frac{e\boldsymbol{E}}{m\omega}[\cos(\omega t - \varphi) - \cos(\varphi)] \\ E_{drift} &= \frac{1}{2}m(\bar{\boldsymbol{v}})^2 = \frac{1}{2m}\left(\frac{e\boldsymbol{E}}{\omega}\right)^2 \cos^2(\varphi) = 2U_p\cos^2(\varphi) \end{aligned} \tag{1}$$

where $\boldsymbol{v}$ is the electron velocity, $\boldsymbol{E}$ and ω are the optical electric field amplitude and frequency respectively, and φ is the phase of the field at which the electron tunnels into the continuum.

From eqns. (1), it is clear that ionization that occurs close to the peak of the oscillation, near $\varphi = \pi/2$, results in electrons with very low energies, while ionization near the nodes of the field yields the maximum electron energy of $2U_p$. Since tunneling ionization has a strongly nonlinear dependence on the electric field strength, the probability of ionization is much greater near the peak of the field, and so one would expect, in the absence of any other effect, a distribution peaked at zero energy, falling off rather sharply, with no electrons having energies greater than the maximum drift velocity $2U_p$.

In Fig. 2, three photoelectron spectra obtained from helium in a 120 fs, 780 nm pulse[44] are shown at different intensities, moving progressively further into the tunneling regime. The energy has been plotted in units of the ponderomotive potential, and the three curves have been normalized in order to compare their shapes. In all three curves, it is clear that most of the electrons generated have energies below $2U_p$, the high-energy tail possessing less than 1% of the distribution even at the lowest intensity shown. At this intensity, where $\gamma = 0.7$, the high-energy electrons may be attributed to the fact that multiphoton processes are still contributing to the ionization. As the intensity increases, the high-energy tail drops precipitously, as expected in the tunneling regime. However, the highest intensity lies well within the tunneling regime, and here one might expect the high-energy tail to be even lower. In fact, this high-energy electron distribution may be modeled in terms of rescattering.

When an electron returns to the core and scatters off it, its velocity is changed, and it is accelerated again in the optical field. In this case, energies much larger than $2U_p$ can be reached: up to $10U_p$ for electrons scattered through an angle of 180°, and these rescattering electrons account for the high-energy tail of the distribution. In Fig. 2(b), the energy distribution at 0.8 PW cm^{-2} is compared with two rescattering calculations as well as the distribution from tunneling ionization alone. As expected, the tunneling ionization distribution drops out above $2U_p$, while rescattering contributes electrons at higher energies. The distribution depends on the details of the scattering potential: the agreement is made substantially worse by using a simple Coulombic potential instead of the actual He^+ core potential. This sensitivity to the core potential has also been demonstrated in comparative experiments at longer wavelength with alkali atoms.[45] The provenance of the high-energy electrons from rescattering is also supported by changes in the angular distribution: below $2U_p$ they are sharply peaked, consistent with tunneling ionization, while above $2U_p$ they become broader.[44]

The last strong field atomic effect that we consider is the correlated emission of two electrons from an atom. This is often called *nonsequential* double ionization, as opposed to the simple, sequential ionization of the neutral followed by the independent ionization of the remaining ion. This problem has an interesting history: the question of the existence of collective effects in strong field interactions motivated many investigations since the field's beginning (see ref. 9 for a discussion). At first they were believed to be seen in the double ionization of alkaline earth atoms, but this proved to be only under somewhat special cases involving the excitation of doubly excited states.[46,47] In most cases, these doubly excited states autoionize to excited ionic states, but in states in which both electrons possess large angular momentum—'planetary

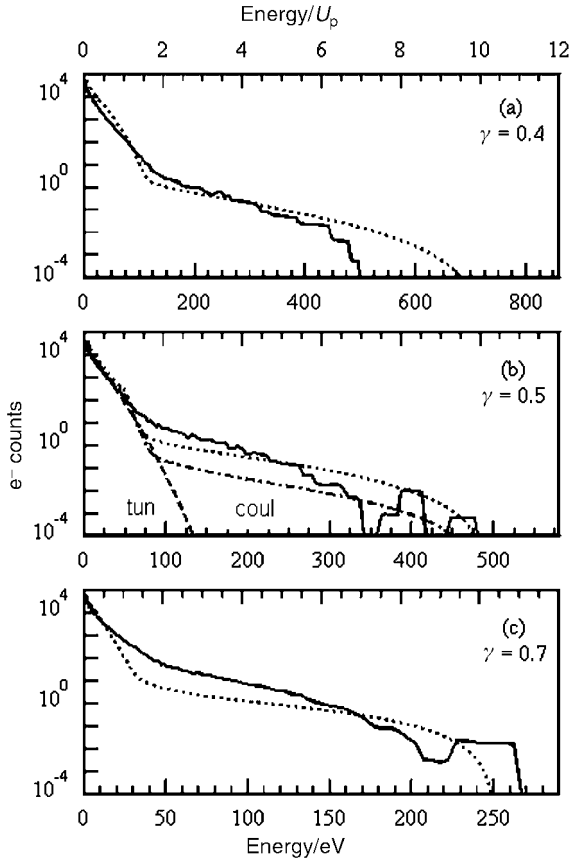

Fig. 2 Experimental (solid lines) helium photoelectron energy distributions for several intensities of a 780 nm, 120 fs laser pulse, compared to rescattering theory (dotted lines). γ is the value of the Keldysh adiabaticity parameter. (a) $I = 1.2$ PW cm^{-2}. (b) $I = 0.8$ PW cm^{-2}. (c) $I = 0.4$ PW cm^{-2}. In (b), the other curves are the theoretical distributions if only tunneling is considered without rescattering (tun), and if rescattering is from a pure Coulombic potential (coul).

double Rydberg states'— the decay to the double continuum can dominate the autoionization rate. The latter case must be specially prepared however; in the more likely former case, although doubly excited states are involved, the ionization is still sequential. The observation of two rates in the intensity dependence of the double ionization of xenon[48] was also long thought to be a signature of nonsequential ionization, until it was shown[49,50] that a sequential path through an excited ionic state explained the double rate.

In helium, two rates are also observed in the double ionization,[2,10,49] as can be seen by the knee structure in the He^{2+} yield curve in Fig. 1. The steep part of the curve above the knee corresponds to sequential ionization, and can be modeled by a TDSE-SAE calculation (solid curve). Below the knee, the rate is orders of magnitude above the sequential rate, and is attributed to a direct, nonsequential double ionization process.

In this case, a process involving intermediate excited ionic states can be ruled out, since at the intensities in the experiment, any excited states would be unbound. Furthermore, it was verified in detail[2] that the knee turns over at the same intensity that the single ionization saturates. That the low-intensity double ionization shuts off as the neutral atom is depleted in the focal volume implies a direct, nonsequential double ionization.

Given the success of the rescattering model in modeling HHG and photoelectron energy spectra, it seems reasonable to expect the process to play a role in double ionization. This has, however, proven to be a rather controversial issue. The first attempt to model the double ionization by inelastic scattering of tunnel-ionized electrons and the ion core[15] used the spread δx of the electron wave packet, which grows between ionization and rescattering, as a free parameter. The value of δx obtained was much smaller than estimates based on time-dependent calculations or elementary arguments however,[2] and if these estimates were used instead, the predicted nonsequential rate would be too low by at least an order of magnitude. A further problem with the rescattering model was the absence of a predicted cutoff: if the returning electron does not have sufficient energy to ionize the core, no double ionization should occur. Since the maximum energy ($3.2U_p$) acquired by the electron from the optical field is proportional to the optical intensity, there should be a well-defined low-intensity cutoff to the nonsequential yield. Even if one defines this intensity assuming that the electron need only excite the core (an excited ion would rapidly ionize in the strong field), there is no evidence for the cutoff in the experimental data.

On the other hand, other details suggest the rescattering picture. The double ionization rate is very sensitive to the optical polarization, dropping precipitously with the introduction of any ellipticity.[2,51,52] Since any ellipticity would give the electron angular momentum, which in turn would tend to make it miss the ion core, this may be taken as supporting a rescattering picture. Furthermore, it has been shown[2] that the double ionization rate is proportional to that part of the single ionization that is due to tunneling. It has been argued that the rate problems with the rescattering model could be resolved by including such effects as refocusing of the electron wave packet by the Coulomb field, multiple electron returns to the core over several optical cycles, and modifications to the inelastic cross section due to the presence of the optical field.[53]

Until recently, the only experimental data available to resolve the issue were in the form of ion yields.[2,10–12] The nonsequential double ionization rate is orders of magnitude smaller than the single ionization rate, so identifying electron spectra associated just with the double ionization is problematic. Recently, several groups have overcome the experimental difficulties. One solution has been to use cold target recoil ion momentum spectroscopy (COLTRIMS), which infers the summed momenta of the two electrons from the momentum of the parent double ion. Double ionization of both helium[54] and neon[55] have been studied with this technique, and both studies indicate that the distribution of electron momenta in double ionization peak at nonzero values. An extension of the technique, which detects electrons in coincidence with the ions, permits the measurement of the electrons' momenta correlation.[56] This was used in a study of argon, and it was found that the two electrons tended to exit on the same side of the ion. These results, along with recent electron–ion coincidence spectroscopy

of helium,[57] also support the rescattering model over other models that have been proposed. Other models, such as shakeoff[10] or collective tunneling are expected to yield electron energy distributions peaked at zero momentum, because all are[58] taken to produce the two electrons within a time short compared to the optical period, and to maximize near the peak of the optical field, producing final electron energies near zero.

The complete answer to the question will probably only come after more extensive experiments are completed in helium, and complete three-dimensional two-electron time-dependent calculations are also completed. The argument as it is currently framed may in fact be something of a false dichotomy, in that coherent effects of the two-electron wave function that persist over several optical cycles may not fit well into any semiclassical interpretation. Other numerical calculations of evolving wave functions offer a hint of what other complications could surface in the problem. For example, in the time-dependent calculations of the single ionization in argon,[59] it is possible to identify in the evolving electron wave function a periodic current away from the core that occurs at the optical frequency. This current may be broken into a bound and an asymptotically free component. The bound component remains closer to the nucleus, and interferences that build up over several cycles have dramatic effects on the ionization. One can imagine a similar process occurring in the two-electron wave function, which could be consistent with the observed momentum distributions, and it would be difficult to interpret it within a semiclassical model involving single discrete emission and re-collision times or in many of the competing theories. The intense field many-body *S*-matrix theory calculation that successfully predicts many of the experimental data[60] is sometimes associated with rescattering[56] because significant contributions to the double ionization rate come from just one Feynman diagram that includes rescattering, but it is important to note that this diagram also includes energy sharing between the electrons that occurs over all time intervals.

It is really the controversy itself that underscores the interest and the value of the double ionization problem. Developing a complete quantitative model of two-electron dynamics, including correlation, has been an important theoretical challenge in which significant progress has recently been made. Nonsequential double ionization is playing the role of the paradigmatic problem by which to test these new models. This is especially true in helium, the simplest two-electron system. As both the theoretical models and the experiments evolve, a clearer picture of correlated two-electron dynamics will emerge.

3 Strong field photodissociation

The additional degrees of freedom in a molecule of course make their interactions with strong optical fields more complex. Still, at very strong fields, a great deal may be understood in terms of phenomena that begin with tunneling ionization, as we will see in the next section. First, we will consider here a broader spectrum of phenomena associated with strong field molecular photodissociation by considering the problem of the dissociation of the hydrogen molecular ion H_2^+.

The fragmentation involves principally only two electronic states: the attractive $1s\sigma_g$ ground state and the first repulsive $2p\sigma_u$ state. In most experiments, the ion

formation and dissociation are accomplished with the same laser pulse, but photoelectron spectra measurements have demonstrated that the molecular ion is formed in vibrational levels of the $1s\sigma_g$,[61–63] while the measured fragment energy distributions show that excitation to the $2p\sigma_u$ is the main dissociation path. It has also been demonstrated experimentally that the ionization and dissociation are sequential.[62–64]

A time-independent theory of the dissociation may be approached in either of two essentially equivalent formulations. In a generalized Floquet theory,[65,66] the optical field is treated classically and the radiative couplings and molecular eigenfunctions expanded in a Fourier series. The interpretation is a little more intuitive in the dressed state picture[67] and we will follow that here.

Then the optical field is treated quantally, in terms of photon number states $|N-n\rangle$, where N is the arbitrarily large number of photons in the field, and n is the number of photons absorbed by the ion. The eigenstates in a product representation, for a basis restricted to our two electronic states, are then

$$\psi(\boldsymbol{r},\boldsymbol{R},N,E)=\sum|N-n\rangle\varphi_{\mathrm{g}}F_{\mathrm{n,g}}(\boldsymbol{R},E)+|N-n\rangle\varphi_{\mathrm{u}}F_{\mathrm{n,u}}(\boldsymbol{R},E)$$

where the φ_i ($\boldsymbol{r}$, $\boldsymbol{R}$) are the field-free electron wave functions for the $1s\sigma_g$ and $2p\sigma_u$ in the Born–Oppenheimer approximation, and the functions $F_{n,i}$ ($\boldsymbol{R}$, E) are the nuclear wave functions. The Hamiltonian comprises those of the bare molecule and optical field, and the coupling between them:

$$H = H_0 + H_{\mathrm{opt}} + V_{\mathrm{int}}$$

In the absence of any coupling ($V_{\mathrm{int}} = 0$), one obtains the diabatic basis—to each bare molecular state there corresponds a ladder of potential curves, each identical to the potential curve in zero field, but shifted in energy by an integral number of photons.

Four of these states are shown in Fig. 3 (solid curves), which is adapted from ref. 67. The dashed curves represent the adiabatic basis for a particular intensity, obtained by truncating the basis and diagonalizing the Hamiltonian as a function of the internuclear separation. Care must be taken in the choice of gauge before doing this however. In the Coulomb gauge [$V_{\mathrm{int}} = (e/Mc)\boldsymbol{p}\cdot\boldsymbol{A}$], the large values of the coupling at small internuclear distances make the restriction to two molecular states unjustified. A comparison with the variational calculations of Muller has demonstrated that the two-state approximation is justified using the length gauge ($V_{\mathrm{int}} = e\boldsymbol{r}\cdot\boldsymbol{E}$).[68,69] The divergence of the coupling at large internuclear separation is not a problem for calculations involving short pulses, as the interaction is over before large separations are reached.

In the figure, the adiabatic curves are calculated for an intensity of 10^{13} W cm^{-2}, and a wavelength of 532 nm, but of course the shape of the curves changes with intensity, and much of the dynamics may be associated with this change in shape. As the intensity increases, the barrier in the ground state potential (g,$n = 0$) is lowered, and vibrational levels lying above the barrier (*e.g.* $v = 12$ in the figure) become unbound, dissociating along the u,$n = 1$ curve. At higher intensities, even the $v = 1$ and $v = 2$ levels become unbound. This process is known as 'bond softening' due to the gradual weakening of the binding potential with intensity.[61]

Paradoxically, it seems possible that, under some circumstances, a higher order (in photon number) process can dominate a lower order process. Consider a lower vibrational level in the g,n = 0 potential well. At lower intensities, dissociation along the u,n = 1 path requires tunneling through a substantial barrier. It is more likely that the molecules pass to the u,n = 3 channel and then go, either diabatically or adiabatically, through the gap at the level crossing with the g,n = 2 channel. With increasing intensity, this gap opens up, the adiabatic passage becomes more likely, and the system dissociates along the g,n = 2 channel. The net absorption is two photons, though the process is really fourth order—three photons absorbed followed by one stimulated emission. By analogy with the ATI in atoms, in which excess photons beyond what is required to reach the ionization limit are absorbed, this process is known as above-threshold dissociation (ATD).[61]

Experimental observation of these effects requires an understanding of the population distribution in the vibrational levels of the ionic ground state. In a long-pulse experiment, *i.e.* one in which the laser pulse is sufficiently long that an electron may leave the focus before the pulse is over, this information can be extracted from the energy spectrum of the photoelectrons produced in the ionization step. This is due to an interesting cancellation of energy shifts that occurs. Intermediate Rydberg states are Stark-shifted by an amount dependent on the instantaneous light intensity at the molecule's position.[70–72] This shift is canceled by an approximately equal ponder-

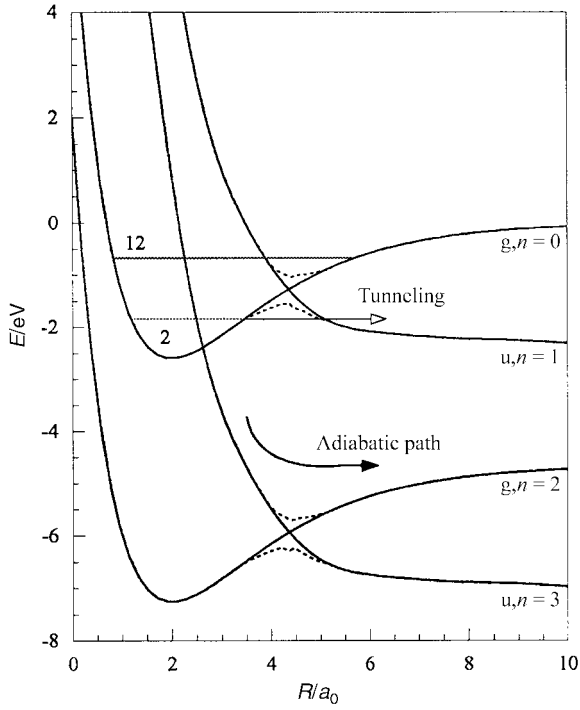

Fig. 3 Diabatic and adiabatic potentials for the $1s\sigma_g$ and $2p\sigma_u$ states of H_2^+, and possible dissociation pathways. Calculated for λ = 532 nm, at an intensity of 10^{13} W cm^{-2}. Adapted from ref. 67.

omotive shift of the ionization threshold. In a short-pulse experiment, these canceling shifts, together with the $\delta v = 0$ propensity rule, tend to wash out vibrational information. In a long-pulse experiment, however, the electron acquires energy equal to the ponderomotive shift as it leaves the laser focus and the vibrational information is restored.

Several photoelectron spectra, from ref. 63, are shown in Fig. 4. Seven photons are required to ionize H_2 at the wavelengths shown (527 and 532 nm), and the two sets of peaks correspond to seven- and eight-photon ionization, with clearly resolved vibrational structure. At the lowest intensities, the Franck–Condon factors for nonresonant absorption predict the vibrational distribution. The shift towards a dominant $v^+ = 0$ population at increased intensity indicates the presence of an intermediate resonance. The resonances can be identified, and though this means there is some spatial inhomogeneity over the focal volume due to intensity variations, the overall vibrational state distribution can be determined. The gradual disappearance with increasing intensity of the peaks corresponding to higher vibrational levels in the

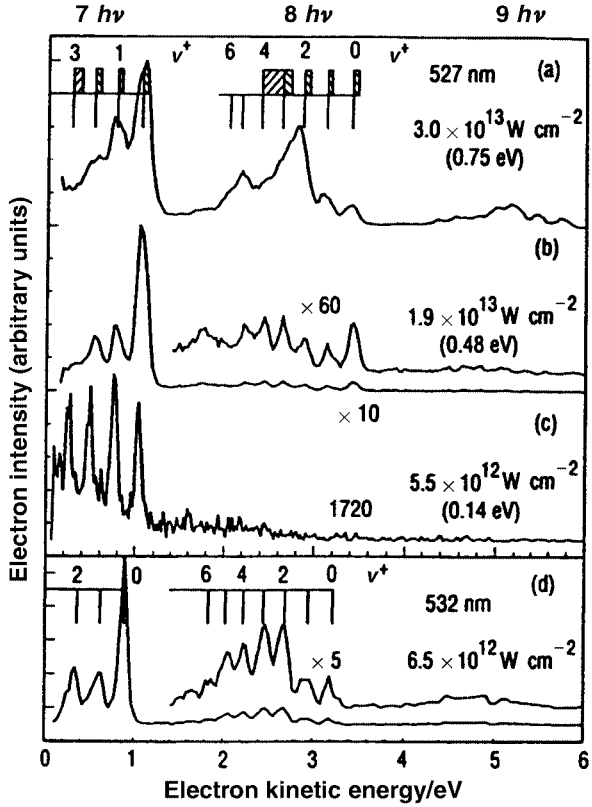

Fig. 4 Photoelectron energy spectra at several intensities for the H_2 molecule in 527 nm and 532 nm optical fields. Peaks are labeled with the vibrational quantum numbers of the H_2^+ molecular ion ground state. Energies in parentheses are the ponderomotive energies at each intensity. Reproduced with permission from ref. 63.

seven-photon peak is just due to the ponderomotive shift of the ionization threshold to higher energy.

Vibrational distributions derived from Fig. 4 are used to calculate the H^+ energy spectrum shown in Fig. 5. The peaks are labeled with the vibrational level of the parent molecular ion, and the theoretical curve is calculated at the peak intensity (1×10^{13} W cm^{-2}), without any spatial or temporal averaging. The dotted curve shows the experimental spectrum. The low-energy peak corresponds to bond softening, while the ions in the higher energy peak dissociated through ATD. While the calculation seems to underestimate the number of ions in higher vibrational states that dissociate through ATD, the overall shape of the predicted distribution is correct. The branching ratio between ATD and bond softening is depicted in Fig. 6, from ref. 63, for both hydrogen and deuterium molecular ions. Two different ion yield ratios are considered for each isotope: the total ATD yield, including both two- and three-photon channels, is compared to the bond softening yield (labeled ATD/1), and the three-photon ATD yield is compared to the two-photon ATD yield (labeled 3/2). The ATD/1 ratio shows an increase with intensity in both isotopes. Since lower vibrational levels might be expected to dissociate preferentially *via* ATD, this result may be explained if the higher vibrational levels are saturated or sensitive to the optical intensity.[69] The flat or decreasing behavior of the 3/2 ratio is to be expected though (see Fig. 3), as ions that have absorbed three photons will preferentially pass adiabatically through the (g,n = 3)–(g,n = 2) anticrossing as the intensity increases and that energy gap widens. This is underscored by the fact that 3/2(H) is much larger than 3/2(D) at the lowest

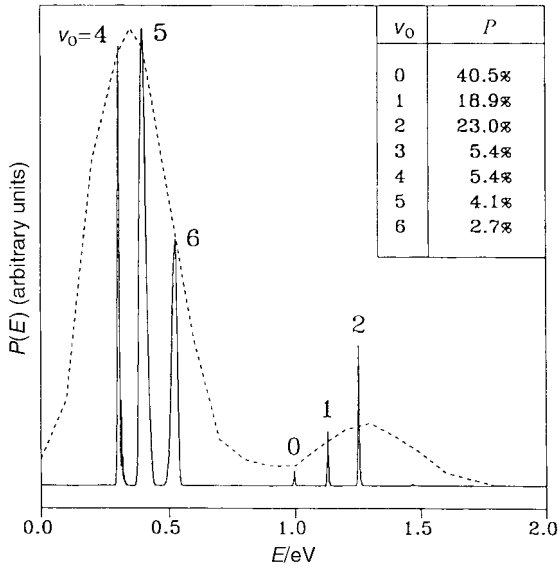

Fig. 5 Experimental (dotted curve) and theoretical (solid curve) H^+ energy spectrum in the dissociation of H_2^+ by a 532 nm, 10^{13} W cm^{-2} peak intensity optical field. The vibrational distribution for the calculation was derived from data in the previous figure.

intensities when the gap is smallest, reflecting the fact that the lower vibrational frequency in D_2^+ would favor adiabatic passage.

One of the most interesting possibilities presented by the intensity-dependent shape of the adiabatic potential curves in Fig. 3 is that of the formation of potential wells deep enough to contain bound vibrational states at large internuclear separation. Since these light-induced bound states (LIBS) exist only for a limited range of optical intensities, it is possible that population becomes 'trapped' in these states during some part of a laser pulse, and remains stable against dissociation until the optical intensity falls again to the point that the adiabatic well can no longer support bound states. Figs. 7 and 8, both from ref. 73, show the formation of the well during the laser pulse, and experimental evidence for the existence of the light-induced states.

In Fig. 7, the changing shape in the potential and the motion of a vibrational wave packet are followed as they evolve in a 1×10^{15} W cm^{-2} peak intensity, 160 fs

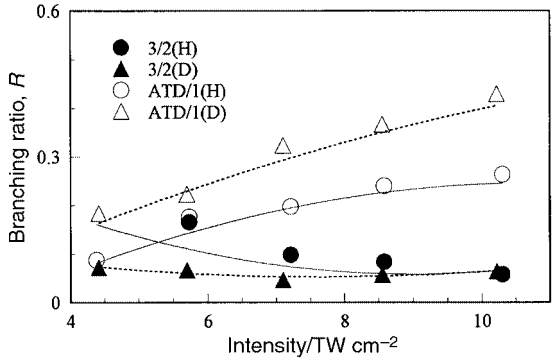

Fig. 6 ATD and bond softening branching ratios as a function of intensity in the dissociation of H_2^+ and D_2^+ at λ = 532 nm. See text for details. Reproduced from ref. 63.

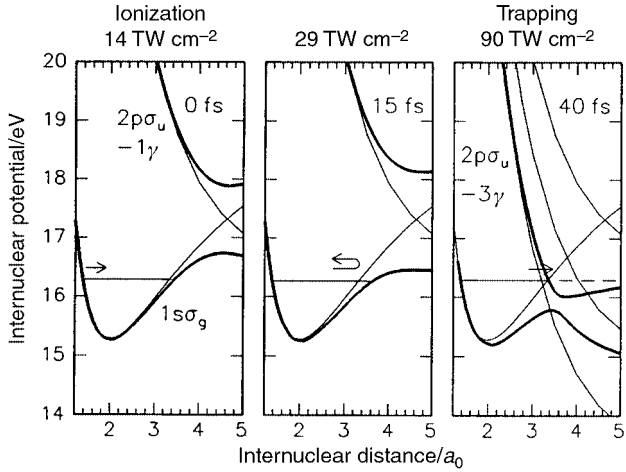

Fig. 7 Motion of a wave packet on the adiabatic potential curves in a laser pulse, illustrating how trapping in a light-induced bound state (LIBS) might occur. Reproduced from ref. 73.

(FWHM) pulse of 769 nm radiation. The clock starts when the wave packet is formed by the ionization of the neutral hydrogen molecule at an intensity of 2.9×10^{13} W cm^{-2}. At the end of one half of a vibrational period, when the wave packet has reached the outer turning point, the one-photon dissociation channel is still closed, and another vibrational cycle occurs. At 40 fs, when the wave packet has returned to this point, the three-photon gap is already open, and there is significant probability of a diabatic transition across the gap, populating vibrational states in the newly formed well in the $2p\sigma_u$.

In fields of this strength, the second electron may also be removed, and the two bare nuclei will fly apart under the strong Coulomb repulsion. If the population survives in the adiabatic well long enough (one vibrational period, or approximately 50 fs) before the second ionization occurs, then the vibrational structure should be manifest in the energy spectrum of the ions. A modulation is seen on the broad high-energy peaks of both the H^+ and D^+ spectra in Fig. 8, with peaks at energies consistent with excitation out of the vibrational levels of the adiabatic potential well. Above the spectra are the calculated Franck–Condon overlaps of the eigenfunctions of these vibrational states with the repulsive Coulomb state.

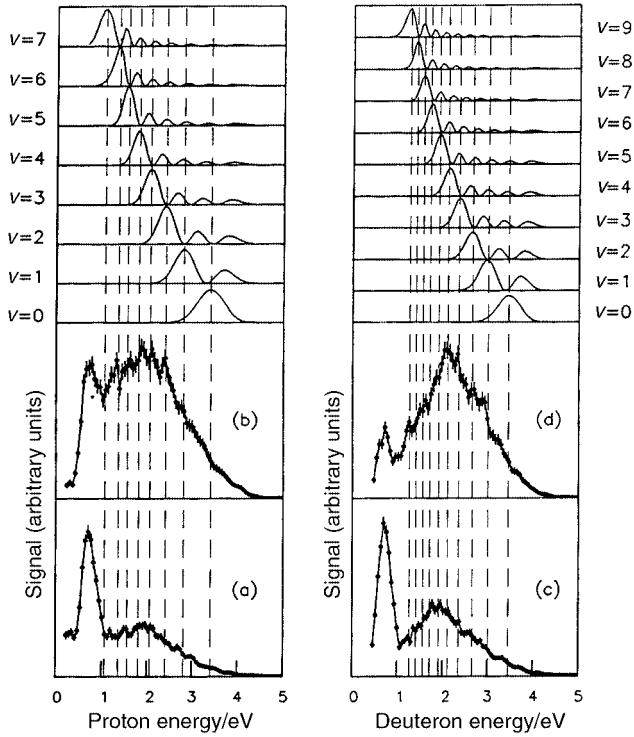

Fig. 8 Energy spectra of H^+ (left) and D^+ (right) from the dissociation of H_2^+ and D_2^+ in a 769 nm optical field at intensities of 1 PW cm^{-2} (a,c) and 2 PW cm^{-2} (b,d). The Franck–Condon overlaps between vibrational levels of the light-induced bound state and the repulsive coulomb state correlate with the modulations in the high-energy peaks. Reproduced from ref. 73.

Because the observed modulation depth in this high-energy peak is small, the identification with LIBS has been controversial. The theoretical support for populating LIBS at pulse lengths as long as 160 fs has been questioned. Yao and Chu[74,75] predict trapping in the three-photon well for a 100 fs pulse, but their calculations freeze the rotational degrees of freedom. Aubanel *et al.*[76] included rotational excitation and found that it destroyed the trapping in the three-photon well, but that higher vibrational levels could be trapped in a well in the one-photon dissociation channel. Numico *et al.*[77] found strong theoretical support for efficient trapping in LIBS at shorter wavelengths with very short ($\leqslant$40 fs) pulses. The experimental evidence was complicated by the finding of Gibson *et al.*[78] that the broad high-energy peak in the ion spectrum alone does not constitute evidence that LIBS have been populated, as had been suggested.[69,73] In an experiment in which the population of LIBS was carefully excluded, they showed that ionic molecules dissociating along the one- and two-photon channels underwent further ionization and that these fragments contributed to the high-energy peak.

There are many factors that broaden and shift the peaks associated with the vibrational structure in Fig. 8,[73] so it is unlikely that the experimental case can be made stronger in the 160 fs pulse regime. Because population trapped in LIBS will dissociate during the relatively long falling edge of the laser pulse, survival probability of the molecular ion cannot be used as an experimental signature. A short-pulse experimental study has recently found strong evidence for the population of LIBS however. Frasinski *et al.*[79] found a shift in the energy of the one-photon dissociation peak, which decreases with increasing pulse width. This can be attributed to trapping of population in an adiabatic well formed near the one-photon–three-photon anticrossing. The population survives through the peak of the pulse, but as the light pulse shuts off, the shape of the potential changes and the well becomes a hill. Some of the population rolls back into the $1s\sigma_g$ bound state and the rest dissociates along the u,n = 1 channel. The energy kick received by the dissociating ions from the changing shape of the potential is larger for faster fall times of the laser pulse, and the predicted pulse width dependence of the energy shift is observed in the experiment.

4 Coulomb explosion

The previous section restricted its treatment to the dissociation of a simple molecule involving a low ionization state. However, in very strong fields, molecular dissociation is often characterized by very high charge states and very energetic ionic fragments. Our understanding of the dynamics of this multi-electron dissociative ionization (MEDI) has an interesting history. At the time that energetic highly charged photofragments were first observed in strong field photodissociation,[80] it was suggested that the intense field removes electrons rapidly from the molecule through field ionization, and that the remaining ions fly apart due to their mutual Coulomb repulsion. As such, the process held great promise, not only as a tool for probing the equilibrium geometry of molecules, but also as an ultrafast probe of the dynamics of photodissociation, the fragments themselves revealing, through their energies, the progressive distortion of the molecule at each stage of ionization.

Subsequent experimental work did not fulfill this hope, but delivered interesting new problems instead. Within this 'Coulomb explosion' interpretation of the process, it appeared that all of the ionization occurred at a critical internuclear separation R_c, which was roughly 40% to 150% larger than the equilibrium bond length R_e. Attention rapidly focused on the feature distinguishing molecules from atoms in strong field ionization: the presence of an internal potential barrier between the potential wells associated with the nuclei. Codling *et al.*[81] recognized that tunneling through the external barriers was not the only route to the continuum, and that the changing height of the internal barrier (see Fig. 9 and discussion below) as a function of internuclear separation might lead to a 'critical distance' at which much of the molecular electronic charge could go over or tunnel through this barrier directly into the continuum. One of the earliest models of this process was a simple but effective treatment in which the electron cloud was treated as a continuous fluid. We shall discuss that first, since, though much of the later work developed the essential physics surrounding the critical separation—the discrete states involved,[82] the dynamics of populating the upper well,[82–85] and quantitative predictions of experimental results[83–85]—problems remain. Also a recent hydrodynamic model,[86–88] which again treats the electrons continuously and has some experimental support,[88] suggests that electrical screening of the repelling ions may be the most important dynamic effect and that the hypothesis of a critical internuclear separation may be unnecessary.

In Fig. 9, taken from ref. 89, the electron potential is plotted along the internuclear axis for a diatomic molecule, N_2, at a peak optical electric field of 10.3 V Å^{-1}. In Brewczyk and Frasinski's Thomas–Fermi–Dirac model, a generalization of the Thomas–Fermi model that includes electron exchange, the shaded region represents the electron cloud, and fills the potential well up to the Fermi energy. The asymptotic slope of the potential alternates between positive and negative on each cycle of the optical field. The molecular charge is not constrained to integral multiples of *e*, and electron transfer occurs both between the potential wells and into the continuum, when the electron cloud spills over the barriers. For a range of internuclear separations [*e.g.* Figs. 9(b) and (c)], the height of the internal barrier is such that transfer from the upper well directly to the continuum happens over the internal barrier. Once charge is lost to

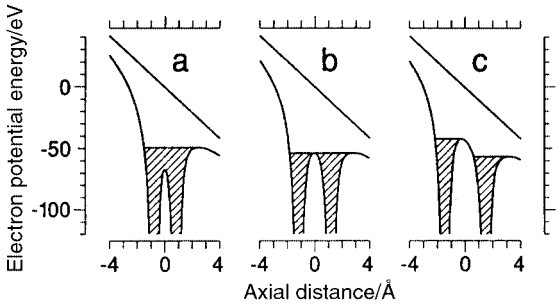

Fig. 9 Potential along the internuclear axis in the TFD model for a nitrogen molecule in a 10.3 V Å^{-1} field at internuclear distances of (a) 1.6 Å, (b) 2.3 Å (the dissociation point) and (c) 3.0 Å. The shading shows the electron population, which fills the wells up to the Fermi energy. Reproduced from ref. 89.

the continuum, both charge centers have a net positive charge, and the Coulomb repulsion drives them further apart. With increased separation, the internal barrier rises higher and, for a given field, there is a separation beyond which transfer over the internal barrier is suppressed. Once ionization has ceased, the Coulomb repulsion between the charge cores determines the final fragment energies.

Fig. 10 shows how the nitrogen molecule dissociating in laser fields of varying strength evolves. Consider the center curve, which represents a peak field of 10.3 V $Å^{-1}$, corresponding to an intensity of 5×10^{15} W cm^{-2}. The solid curve shows the ionization of the minimally ionized molecule (defined to be when the Fermi energy just reaches the top of the barrier) as a function of internuclear separation. The dotted curve represents a molecule that sees the field turned on instantaneously. In the latter case, at the first crest of the field, when the internuclear separation is still at its equilibrium value, the molecule rapidly ionizes to a charge of 3+, and the Coulomb repulsion begins to drive the ions apart. Slightly more charge is removed on each optical cycle, until the dissociation point, indicated by the dashed curve in the figure, is reached, after which charge loss stops and the fragments continue to move apart. Charge transfer between the fragments changes direction on each optical half-cycle and continues up to the point marked in the figure by an asterisk.

This model is reasonably successful, but raises difficulties as well. The highest ionization stage reached in dissociation is predicted well, though thresholds for ionization stages below 3+ are underestimated. The experimentally observed predominance of symmetric fragmentation—dissociation in which the fragments differ in charge by one unit or less—is also predicted: the transfer between wells that continues beyond the dissociation point tends to equalize the charge on the fragments. Its prediction of a critical internuclear separation (the dissociation point in Fig. 10) larger than R_e is also consistent with experiment, but it underestimates the ionization enhancement that occurs there (see below).

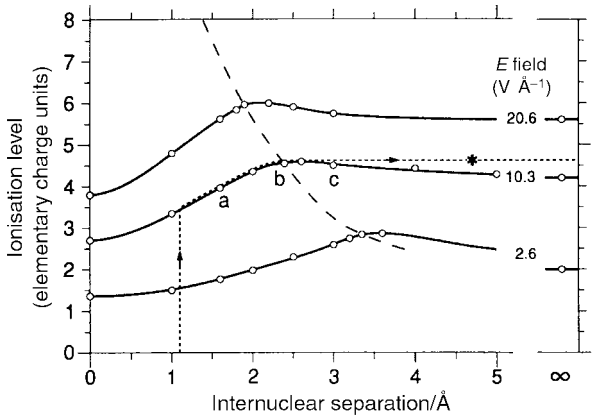

Fig. 10 The solid curves show the ionization level of an N_2 molecule *vs.* internuclear separation for several fields in the TFD theory. The dotted line maps the evolution of a molecule suddenly exposed at R_e to a 10.3 V $Å^{-1}$ field. The lettered points correspond to the potentials in the previous figure. The dashed curve indicates the dissociation point, and the asterisk is the point beyond which charge transfer between potential wells ceases. Reproduced from ref. 89.

One would expect from this picture that lower charge states would form at smaller internuclear separation, closer to R_e, than higher charge states. However, this turns out not to be the case. Schmidt *et al.*[90] found, in their studies of the dissociation of Cl_2, that the value of R_c inferred from the fragment energies was the same for all fragmentations channels of the molecule, up to a charge state of 8+. In an analysis of their own experiment and previous experiments on seven other molecules, they found a strong correlation between R_c and R_e. For chlorine, the equilibrium bond length is 2 Å, and the observed fragment energy is 70% of the energy that would result from a fragmentation at R_e, implying $R_c/R_e \sim 1.4$. In the molecules H_2, N_2, O_2, CO, C_2H_2, and CO_2, the equilibrium bond length is shorter (1.1–1.2 Å), while the fragment energy lies between 40% and 50% of that of a fragmentation at R_e, or $R_c/R_e \sim 2.0$ to 2.5. The authors find an empirical scaling law of $R_c = 2.3\sqrt{R_e}$ (lengths in Å) that is molecule-independent.

In pulses of approximately 100 fs and longer—up to several picoseconds—there appears to be little dependence of either the fragment energies or fragmentation branching ratios on the pulse length or wavelength.[90,91] This implies that the bond elongation to R_c occurs very quickly. It also suggests that the molecule is stabilized near R_c over much of the pulse in the picosecond pulses, as no postdissociation ionization of the fragments is observed.[90] At shorter pulse lengths, especially below ~30 fs, the dynamics does seem to change substantially. Ionization does occur at bond lengths smaller than R_c,[92–95] and charge-asymmetric dissociation channels and excited fragment states become important.[92–94,96] We will not discuss this ultrashort-pulse regime at length here, but it should be noted that in this regime the original hope of using the Coulomb explosion to take a snapshot of a molecule at an instant of time may be fulfilled. The current state of laser technology affords pulses shorter than 5 fs,[97] sufficient to cause the probability of dissociating a molecule to go from 0 to 1 within the space of half of an optical cycle.[98] In conjunction with the rapidly developing technique of timed Coulomb explosion imaging,[98–100] this may permit the detailed tracking of the evolution of molecular wave packets on femtosecond time scales.

Several theoretical studies have predicted the ionization enhancement that occurs at R_c, and clarified the physics underlying it.[82–85,101] Time-dependent calculations have shown that charge transfer states play an important role in the dynamics,[82] and that it is the nonadiabatic response of the electrons to the oscillating electric field which engenders the population of the upper potential well that subsequently feeds population to the continuum across the internal barrier.[82–85] The resulting enhancement of the ionization rate at R_c is an order of magnitude larger than the neutral molecule (it is because the TFD model assumes that the electron cloud adiabatically follows the field that it underestimates the enhancement). Both the magnitude of the enhancement and the range of values obtained for R_c are in good agreement with experiment.

The importance of a critical separation in several theories makes the recent proposal of a hydrodynamic model[86–88] in which such a separation is absent something of a surprise. Yet the model has now successfully predicted experimental results in one diatomic (Cl_2)[86] and two triatomic molecules (CO_2 and N_2O),[88] and offers some very new insights into the problem. One advantage of the model is that it considers the motion of all of the electrons. It is able to handle this by using time-dependent density functional theory instead of trying to solve for the wave function of the many-electron

Schrödinger equation. The electron density evolves under the combined forces of the electrostatic potential due to the ions and electrons, the optical field, and a pressure based on the Thomas–Fermi model, in which the electron cloud is treated as a Fermi gas in which the available phase space is filled subject to the Pauli exclusion principle. It is only in the last term that quantum mechanics even enters the problem. The time evolution of the molecule is treated by simultaneously solving the hydrodynamic equations for the electron density and Newton's equations for the nuclear motion.

Fig. 11, taken from ref. 86, shows the calculated evolution of a Cl_2 molecule in an optical field with a wavelength of 610 nm, a peak intensity of 1.3×10^{15} W cm^{-2}, and a temporal envelope given by $\sin^2 [\pi t/(2\tau)]$, where the rise time τ is 10 optical cycles (20 fs). The arrows on the *x*-axes indicate the time (in optical periods *T*) at which the peak optical field is reached. In Fig. 11(a), the instantaneous kinetic energy of one ion is plotted, while in the inset the nuclear separation as a function of time is shown. The

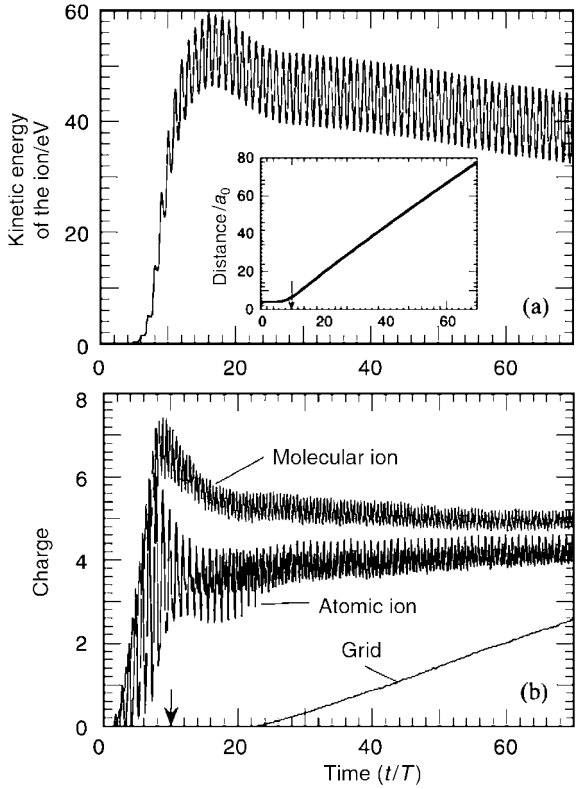

Fig. 11 Evolution of charge and energy in the hydrodynamic model of MEDI for Cl_2 dissociating in a 610 nm optical field with peak intensity of 1.3×10^{15} W cm^{-2}. (a) Kinetic energy of the atomic ion fragments *vs.* time; the inset shows the internuclear separation *vs.* time. (b) Distribution of net charge on the atomic and molecular ions and on the spatial grid containing the calculation (see text). Reproduced with permission from ref. 86.

nuclei remain virtually at rest at R_e until just before the peak field is reached, and then begin to move apart due to the Coulomb repulsion. The charge evolution is shown in Fig. 11(b): the 'atomic ion' curve is the charge enclosed within three atomic units of either ion, while the 'molecular ion' curve indicates the sum of the charges on both ions and all of the charge in between. The 'grid' curve represents the net charge on the spatial grid to which the problem has been constrained—charge is absorbed when it reaches the boundary. Substantial ionization occurs while the ions are still at their equilibrium separation, and shortly thereafter—about $10T$ later—the kinetic energy reaches its maximum. The ions then begin to decelerate. This is the result of a screening of the ionic repulsion due to electrons that lie between the two fragments. The molecular charge shows a sharp decrease after $t \approx 10T$; this is due to the cessation of ionization, and an increase of the enclosed charge due to the increased distance between the ions. Note that both the molecular charge and the atomic charge have settled close to their asymptotic values by about $t \approx 20T$. The charge localized on an individual ion is 4+, but the molecular charge is only 5+, indicating that −3 units of charge lie between the two ions, screening their repulsion.

The energy defect—the difference between the final fragment kinetic energy and the energy that would obtain under Coulomb repulsion from an initial separation of R_e—is in agreement with experiment. A two-dimensional generalization of the model has also been worked out and applied to the triatomic molecules N_2O and CO_2,[88] obtaining agreement on energy defects for ionization states up to 9+.

The connection between the hydrodynamic model and other models remains an open question. Some unanswered questions remain in the critical-distance theories though. It appears that MEDI occurs on time scales faster than a vibrational period, so that it is questionable that bond elongation to R_c can occur fast enough to be important dynamically.[86] In any case, the dynamics of the elongation still need to be quantified. The suggested stabilization against ionization in long-pulse experiments discussed above is also not seen in the hydrodynamic model, and may also provide a test in experiments at higher intensities, where the hydrodynamic model predicts stronger postdissociation ionization.[86] A recent study of the polarization dependence of MEDI[102] may also provide a test discriminating between the theories.

5 Coherent control of dissociation

The proposal by Brumer and Shapiro[26] that interferences created by multiple frequencies coupling quantum states be used to control photochemical reactions coherently went for a considerable time without experimental realization. The first experiments were in atomic systems, in which the relative phase between two harmonic optical fields was used to modulate the coupling between bound states.[27–29] Closer to real chemical control, control in bound–continuum transitions was demonstrated in photoionziation of atoms[30–33] and molecules,[34] and in semiconductors.[39,40] Actual control of fragmentation in a photodissociation process was first demonstrated in hydrogen[35] and CH_3I.[36]

The first demonstration of control in which different reaction products manifested different phase behaviors (thus permitting the manipulation of branching ratios) was accomplished in the photoionization and photodissociation of HI and DI by Zhu *et*

al.[37] Fig. 12, taken from ref. 38, is an example of their data, showing the modulation in yield of the molecular and atomic ions. The *x*-axis is the pressure in a hydrogen cell through which both 354 nm light and its third harmonic copropagate before reaching the interaction chamber. The relative phase φ between the two optical fields is determined by the pressure in the cell and the wavelength dependence of the refractive index of hydrogen. Both ion yields modulate with the periodicity of φ, but there is a pronounced phase lag ($\sim 150°$) between them. By setting the optical phase, one can then preferentially produce either ion from the reaction. As in the case of optimal control, the goal of manipulation, once reached, has in turn produced a remarkable analytical tool: the study of this phase lag has proved to be a powerful tool for probing molecular dynamics.[103–106]

In this section, we will consider the example of coherent control in the simpler system of hydrogen. Two-color phase-control experiments on molecular hydrogen ions have been carried out at two different laser wavelengths, at short and long pulse durations. In the long-pulse experiments,[35] a 50 ps pulse of 1 μm radiation and its second harmonic are used to dissociate HD^+ and H_2^+. In the short-pulse experiments,[107] an 85 fs pulse was used to dissociate H_2^+, and a fundamental wavelength of 750 nm and its second harmonic were used. There was some difference in the dissociation mechanisms in the two experiments, as the combined optical intensity in the long-pulse experiments was $\approx 2 \times 10^{13}$ W cm^{-2}, while in the short-pulse experiments it was $\approx 10^{14}$ W cm^{-2}.

In both experiments, the second harmonic was generated by frequency doubling the fundamental in a BBO crystal, to insure phase coherence between the two colors. The relative phase φ was adjusted either by changing the length of a dispersive material (glass) through which the two colors propagated (long-pulse experiments), or by separating the two colors in a Michelson interferometer, and varying the length of one arm (short-pulse experiments). The two-color pulse is focused into a chamber containing the hydrogen gas, and ion energies are measured using time-of-flight detection. A weak extraction field is applied in the interaction region, both to facilitate ion collection and to discriminate between 'forward' ions (those emitted towards the detector) and 'backward' ions (those emitted in the opposite direction). Backward ions

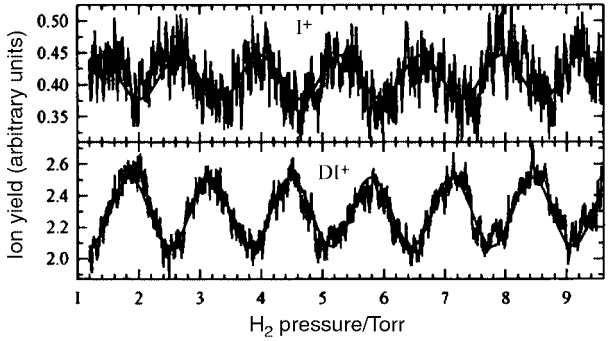

Fig. 12 Modulation of I^+ and DI^+ yields produced by the coherent control of the photoionization and photodissociation of DI. Varying the H_2 pressure in the cell varies the relative phase between the 354 nm radiation and its third harmonic. Reproduced with permission from ref. 38.

are turned around in the extraction field, and so arrive at the detector with a delay relative to the forward ions that is determined by their initial energies and the extraction field strength.

Time-of-flight spectra from the long-pulse dissociation of HD^+, taken from ref. 35, for several values of φ are shown in Fig. 13. The intensity of the fundamental and second harmonic are the same, equal to 1×10^{13} W cm^{-2}. The spectra are expanded about the H^+ and D^+ peaks. Ions with zero kinetic energy arrive at the center of each mass peak; forward ions arrive earlier and backward ions later. The D^+ spectra have an additional contribution to the zero-energy peak due to a small (2%) H_2 contamination in the sample gas; this ionizes to form H_2^+ with a thermal velocity distribution. The forward and backward fragment distribution peaks at an energy of 0.5 eV, indicating that the predominant dissociation pathway is bond softening.[61] ATD produces less than 5% of the yield.

There is a clear modulation of the forward/backward asymmetry of the ion ejection direction with the optical phase. The parameter β, defined as the ratio of the forward ion yield over the backward ion yield, is plotted in Fig. 14(a), taken from ref. 35. A time-dependent calculation by Charron *et al.*,[108] shown in Fig. 14(b), includes the interference between couplings of all photon orders, and although it is calculated for a much shorter pulse width and includes no intensity averaging, it reproduces the modulation.

It is interesting to consider this process in terms of some of the simple semiclassical pictures discussed in the previous sections. In Figs. 13 and 14, the two-color electric field as a function of time is shown for several values of φ. The electric field is positive when it points in the forward (towards the detector) direction. The periodicity of the forward/backward ion ejection asymmetry is, of course, equal to that of the field asymmetry. However, β is a maximum when the field maximum is pointing away from the detector and a minimum when the field maximum points towards the detector. In a naïve interpretation, one might expect just the opposite. During the dissociation of

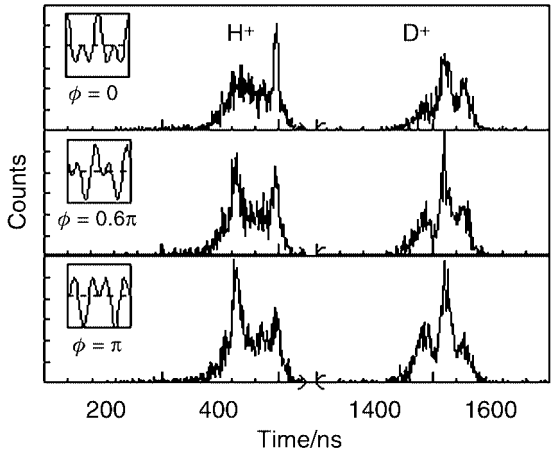

Fig. 13 Time-of-flight spectra at several phases for H^+ and D^+ in the coherent control of the photodissociation of HD^+. The insets depict the electric field as a function of time at each phase shown. Reproduced with permission from ref. 35.

the aligned molecular ion, the larger displacement of the electron in the direction opposite to the electric field maximum would tend to leave the positively charged fragment on the same side as the field maximum. This is certainly a very simple view—the dissociation occurs over several optical cycles so, while the electron displacement is larger on the side opposite the field maximum, it will also be found on the other side as well. However, it does seem surprising that the experimental results are exactly opposite to the intuitive expectation.

The time-dependent quantum mechanical model correctly predicts the counter-intuitive direction of emission. Since the ion ejection asymmetry arises from interferences of different photon order couplings, its relationship to the electric field is a function of the frequencies and intensities in the two-color optical field. At shorter wavelengths, the asymmetry is counterintuitive, but this can change at longer wavelengths. In fact, at longer wavelengths there is a phase lag between the H^+ and D^+ forward/backward asymmetries. For example, at 10.6 μm, this phase lag can be made 180° and the process effectively becomes an isotope separator,[109] with all deuterium ions going in one direction and the hydrogen ions going in the opposite direction for a given value of φ.

In the short-pulse experiments, all three dissociation channels (bond softening, ATD, and Coulomb explosion) are observed. A phase-dependent asymmetry is observed in the $H + H^+$ ATD channel. Both the electrons and the ions were collected

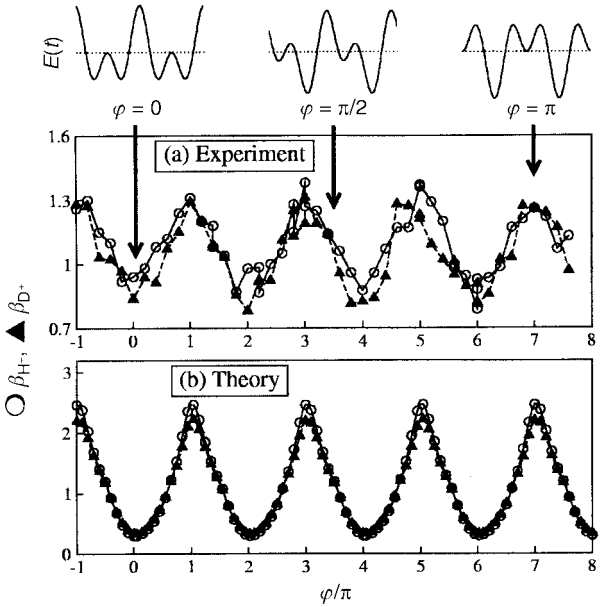

Fig. 14 Forward/backward ion yield ratio β for H^+ (open circles) and D^+ (full triangles). (a) Experimental values in the long-pulse (50 ps) experiment (see text). From ref. 35. (b) Results of a time-dependent calculation with the same wavelength and intensities as the experiment, but with a 0.5 ps pulse.[108] Upper curves show the optical electric field *vs.* time at selected phases between the fundamental and second harmonic.

in this experiment and both ions and electrons were preferentially ejected towards the direction opposite the field maximum. Thompson *et al.*[107,110] propose a different mechanism for the counterintuitive direction of ion emission, which is related to the critical-distance theories discussed in the previous section. In their model, the nuclei begin to separate through either bond softening or some other excitation. While the internuclear distances R are small, the electron moves freely between the nuclei under the action of the oscillating optical field. As R passes the critical separation R_c and the internal barrier between the nuclei rises above the electron energy, no further transfer can occur, and the electron is localized on one of the nuclei. It is the direction of the electric field at the time that R exceeds R_c that determines on which nucleus the electron will be localized. Thus when the electric field maximum points in the forward direction (*e.g.* at $\varphi = 0$), the field actually points in the backward direction for a longer fraction of the optical cycle, making localization of the electron on the nucleus on the forward side more likely. The positive ion then leaves the reaction moving in the backward direction.

The authors used this picture to develop a model,[110] approximating the electronic wavefunction near R_c as a linear combination of two 1s orbitals, each centered on one of the dissociating nuclei. Using a variational method, the electronic energy in a fixed electric field was minimized and the adiabatic distribution of charge over the two nuclei determined as a function of the field strength. The distribution was averaged over one cycle of the optical field to determine the probability of localization of the electron on each nucleus. This method was applied to the long-pulse HD^+ dissociation experiments, and used to calculate the relative intensity dependence of the modulation depth of the forward/backward asymmetry β. The results are shown in Fig. 15, from ref. 110. The agreement is only qualitative possibly because the conditions of the model are incompletely satisfied in the experiment. In the experiment, the projected transit time across the critical distance is approximately one half of an optical cycle, while the time averaging in the model requires that the time be one cycle or more. It

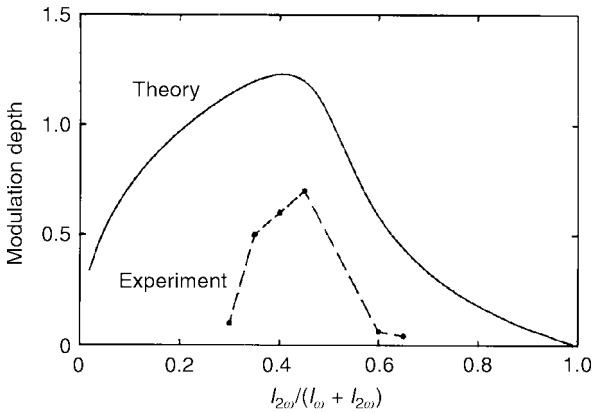

Fig. 15 Depth of modulation of the forward/backward asymmetry β as a function of the relative intensities of the fundamental and the second harmonic in the two-color optical field. The connected dots are the experimental values; the solid line is the model of Posthumus *et al.* Reproduced with permission from ref. 110.

has been suggested[110] that this model would give different predictions than the time-dependent calculations of Charron *et al.*[109] under some conditions. An experimental test discriminating between them might shed light both on two-color dissociation processes and on critical-distance models of Coulomb explosions, but as yet no such test has been performed.

6 Conclusion

The role of intense field interactions in atomic physics and physical chemistry has grown remarkably in the last decade, paralleling the developments in short-pulse laser technology. As the technology enables us to reach shorter time scales and larger fields, the scientific landscape has broadened and the potential applications have multiplied. Even the simplest atomic dynamics in strong fields continue to pose challenging questions and provide important paradigms in developing our ability to model electron correlation and exotic systems. Molecule–field interactions have proven to possess a rich complexity: a new regime in which the optical field can literally change the shape of the dynamics on femtosecond time scales. The physics of just a simple pulse dissociating a molecule has revealed new structures, and challenges our understanding of fundamental processes. At the same time, the possibility of exploiting these structures and the degree of control over the optical field attainable in ultrashort-pulse systems has moved us closer to the ability to engineer chemical reactions at the level of electronic wave functions.

Acknowledgements

This work is supported by the U.S. Department of Energy at Brookhaven National Laboratory under contract DE-AC02-98CH10886, with the support of the Office of Basic Energy Sciences.

References

1 P. Agostini, G. Fabre, G. Petite and N. K. Rahman, *Phys. Rev. Lett.*, 1979, **42**, 1117.
2 B. Walker, B. Sheehy, L. F. DiMauro, P. Agostini, K. J. Schafer and K. C. Kulander, *Phys. Rev. Lett.*, 1994, **73**, 1227.
3 M. Ferray, A. L'Huillier, X. F. Li, L. A. Lompre, G. Mainfray and C. Manus, *J. Phys. B*, 1988, **21**, L31; A. McPherson, G. N. Gibson, H. Jara, U. Johann, T. S. Luk, I. A. McIntyre, K. Boyer and C. K. Rhodes, *J. Opt. Soc. Am. B*, 1987, **4**, 595.
4 Z. H. Chang, A. Rundquist, H. Wang, I. Christov, M. M. Murnane and H. C. Kapteyn, *IEEE J. Sel. Top. Quantum Electron.*, 1998, **4**, 266; C. Spielmann, C. Kan, N. H. Burnett, T. Brabec, M. Geissler, A. Scrinzi, M. Schnürer and F. Krausz, *IEEE J. Sel. Top. Quantum Electron.*, 1998, **4**, 249.
5 G. Farkas and C. Toth, *Phys. Lett. A*, 1992, **168**, 447.
6 S. E. Harris, J. J. Macklin and T. W. Hansch, *Opt. Commun.*, 1993, **100**, 487.
7 Ph. Antoine, A. L'Huillier and M. Lewenstein, *Phys. Rev. Lett.*, 1996, **77**, 1234.
8 K. J. Schafer and K. C. Kulander, *Phys. Rev. Lett.*, 1997, **78**, 638.
9 L. F. DiMauro and P. Agostini, *Adv. At. Mol. Opt. Phys.*, 1995, **35**, 79.
10 D. N. Fittinghoff, P. R. Bolton, B. Chang and K. C. Kulander, *Phys. Rev. Lett.*, 1992, **69**, 2642.
11 S. Larochelle, A. Talebpour and S. L. Chin, *J. Phys. B*, 1998, **31**, 1201; A. Talebpour, C. Y. Chien, Y. Liang, S. Larochelle and S. L. Chin, *J. Phys. B*, 1998, **30**, 1721; S. Augst, A. Talebpour, S. L. Chin, Y. Beaudoin and M. Chaker, *Phys. Rev. A*, 1995, **52**, R917.
12 Th. Weber, M. Weckenbrock, A. Staudte, L. Spielberger, O. Jagutzki, V. Mergel, F. Afaneh, G. Urbasch, M. Vollmer, H. Giessen and R. Dörner, *J. Phys. B*, 2000, **33**, L127.

13 H. B. van Linden van den Heuvell and H. G. Muller, in *Multiphoton Processes–1988*, ed. S. J. Smith and P. L. Knight, Cambridge University Press, Cambridge, 1988, p. 25.
14 K. J. Schafer, B. Yang, L. F. Di Mauro and K. C. Kulander, , *Phys. Rev. Lett.*, 1993, **70**, 1599.
15 P. B. Corkum, *Phys. Rev. Lett.*, 1993, **71**, 1994.
16 L. J. Frasinski, K. Codling, P. A. Hatherly, J. Barr, I. N. Ross and W. T. Toner, *Phys. Rev. Lett.*, 1987, **58**, 2424.
17 D. J. Tannor and S. A. Rice, *Adv. Chem. Phys.*, 1988, **70**, 441.
18 J. L. Herek, A. Materny and A. H. Zewail, *Chem. Phys. Lett.*, 1994, **228**, 15.
19 T. Baumert and G. Gerber, *Isr. J. Chem.*, 1994, **34**, 103.
20 A. P. Peirce, A. Dahleh and H. Rabitz, *Phys. Rev. A*, 1988, **37**, 4950.
21 C. J. Bardeen, V. V. Yakovlev, K. R. Wilson, S. D. Carpenter, P. M. Weber and W. S. Warren, *Chem. Phys. Lett.*, 1997, **280**, 151.
22 V. V. Yakolev, C. J. Bardeen, J. Che, J. Cao and K. R. Wilson, *J. Chem. Phys.*, 1998, **108**, 2309.
23 D. Meshulach and Y. Silberberg, *Nature*, 1998, **396**, 239.
24 A. Assion, T. Baumert, M. Bergt, T. Brixner, B. Kiefer, V. Seyfried, M. Strehle and G. Gerber, *Science*, 1998, **282**, 919.
25 For a concise review of the field's scope and applications, see: H. Rabitz, R. de Vivie-Riedle, M. Motzkus and K. Kompa, *Science*, 2000, **288**, 824.
26 P. Brumer and M. Shapiro, *Chem. Phys. Lett.*, 1986, **126**, 541; P. Brumer and M. Shapiro, *Acc. Chem. Res.*, 1989, **22**, 407; M. Shapiro, J. W. Hepburn and P. Brumer, *Chem. Phys. Lett.*, 1988, **149**, 451.
27 C. E. Chen and D. S. Elliott, *Phys. Rev. Lett.*, 1990, **64**, 507.
28 C. E. Chen and D. S. Elliott, *Phys. Rev. Lett.*, 1990, **65**, 1737.
29 S. M. Park, S-P. Lu and R. J. Gordon, *J. Chem. Phys.*, 1991, **94**, 8622.
30 H. G. Muller, P. H. Bucksbaum, D. W. Schumacher and A. Zavriyev, *J. Phys. B*, 1990, **23**, 2761.
31 Y.-Y. Yin, C. E. Chen, D. S. Elliott and A. V. Smith, *Phys. Rev. Lett.*, 1992, **69**, 2353.
32 N. B. Baranova, I. M. Beterov, B. Y. Zel'dovich, I. I. Ryabtsev, A. N. Chudinov and A. A. Shul'ginov, *JETP Lett.*, 1992, **55**, 439.
33 D. W. Schumacher, F. Weihe, H. G. Muller and P. H. Bucksbaum, *Phys. Rev. Lett.*, 1994, **73**, 1344.
34 V. D. Kleiman, L. Zhu, X. Li and R. J. Gordon, *J. Chem. Phys.*, 1995, **102**, 5863.
35 B. Sheehy, B. Walker and L. F. DiMauro, *Phys. Rev. Lett.*, 1995, **74**, 4799.
36 V. D. Kleiman, L. Zhu, J. Allen and R. J. Gordon, *J. Chem. Phys.*, 1995, **103**, 10800.
37 L. Zhu, V. Kleiman, X. Li, S. Lu, K. Trentelman and R. J. Gordon, *Science*, 1995, **270**, 77.
38 L. Zhu, S. Kunihiro, J. A. Fiss, R. Wada, T. Seideman and R. J. Gordon, *Phys. Rev. Lett.*, 1997, **79**, 4108.
39 E. Dupont, P. B. Corkum, H. C. Liu, M. Buchanan and Z. R. Wasilewski, *Phys. Rev. Lett.*, 1995, **74**, 3596.
40 A. Hachè, Y. Kostoulas, R. Atanasov, J. L. P. Hughes, J. E. Sipe and H. M. van Driel, *Phys. Rev. Lett.*, 1997, **78**, 306.
41 L. V. Keldysh, *Zh. Eksp. Teor. Fiz.*, 1964, **47**, 1945 [*Sov. Phys. JETP*, 1965, **20**, 1307].
42 K. C. Kulander, *Phys. Rev. A*, 1987, **36**, 445; K. C. Kulander, *Phys. Rev. A*, 1987, **36**, 2726; K. C. Kulander, *Phys. Rev. A*, 1988, **38**, 778.
43 M. V. Ammosov, N. B. Delone and V. P. Krainov, *Sov. Phys. JETP*, 1986, **64**, 1191.
44 B. Sheehy, R. Lafon, M. Widmer, B. Walker, L. F. DiMauro, P. A. Agostini and K. C. Kulander, *Phys. Rev. A*, 1998, **58**, 3942.
45 M. B. Gaarde, K. J. Schafer, K. C. Kulander, B. Sheehy, Dalwoo Kim and L. F. DiMauro, *Phys. Rev. Lett.*, 2000, **84**, 2822.
46 X. Tang, T. N. Chang, P. Lambropoulos, S. Fournier and L. F. DiMauro, *Phys. Rev. A*, 1993, **41**, 5265.
47 S. Cohen, P. Camu and A. Bolovinos, *J. Phys. B*, 1993, **26**, 3783.
48 A. L'Huillier, L. A. Lompre, G. Mainfray and C. Manus, *Phys. Rev. A*, 1983, **27**, 2503.
49 B. Walker, E. Mevel, B. Yang, P. Breger, J. P. Chambaret, A. Antonetti, L. F. DiMauro and P. Agostini, *Phys. Rev. A*, 1993, **48**, R894.
50 D. Charalambidis, P. Lambropoulos, H. Schröder, O. Faucher, H. Xu, M. Wagner and C. Fotakis, *Phys. Rev. A*, 1994, **50**, R2822.
51 P. Dietrich, N. H. Burnett, M. Yu. Ivanov and P. B. Corkum, *Phys. Rev. A*, 1994, **50**, R3585.
52 L. F. DiMauro and P. A. Agostini, *Adv. At. Mol. Opt. Phys.*, 1995, **35**, 79.
53 T. Brabec, M. Yu. Ivanov and P. B. Corkum, *Phys. Rev. A*, 1996, **54**, 2551.
54 Th. Weber, M. Weckenbrock, A. Staudte, L. Spielberger, O. Jagutzki, V. Mergel, F. Afaneh, G. Urbasch, M. Vollmer, H. Giessen and R. Dörner, *Phys. Rev. Lett.*, 2000, **84**, 443.
55 R. Moshammer, B. Feuerstein, W. Schmitt, A. Dorn, C. D. Schröter, J. Ullrich, H. Rottke, C. Trump, M. Wittmann, G. Korn, K. Hoffmann and W. Sandner, *Phys. Rev. Lett.*, 2000, **84**, 447.
56 Th. Weber, H. Giessen, M. Weckenbrock, G. Urbasch, A. Staudte, L. Spielberger, O. Jagutzki, V. Mergel, M. Vollmer and R. Dörner, *Nature*, 2000, **405**, 658.
57 R. Lafon, J. L. Chaloupka, B. Sheehy, L. F. DiMauro, P. M. Paul, P. A. Agostini and K. C. Kulander, *Phys. Rev. Lett.*, 2001, **86**, 2762.
58 U. Eichmann, M. Dörr, H. Maeda, W. Becker and W. Sandner, *Phys. Rev. Lett.*, 2000, **84**, 3550.

59 H. G. Muller, *Opt. Express*, 2001, **8**, 44. The reader may view video clips of these calculations on the internet at http://epubs.osa.org/opticsexpress/
60 A. Becker and F. H. M. Faisal, *J. Phys. B*, 1996, **29**, L197; F. H. M. Faisal and A. Becker, *Laser Phys.*, 1997, **7**, 684; A. Becker and F. H. M. Faisal, *Phys. Rev. Lett.*, 2000, **84**, 3546.
61 P. H. Bucksbaum, A. Zavriyev, H. G. Muller and D. W. Schumacher, *Phys. Rev. Lett.*, 1990, **64**, 1883.
62 A. Zavriyev, P. H. Bucksbaum, H. G. Muller and D. W. Schumacher, *Phys. Rev. A*, 1990, **42**, 5500.
63 B. Yang, M. Saeed, L. F. DiMauro, A. Zavriyev and P. H. Bucksbaum, *Phys. Rev. A*, 1991, **44**, R1458.
64 D. Normand, L. A. Lompre and C. Cornaggia, *J. Phys. B*, 1992, **25**, L497.
65 S.-I. Chu, *J. Chem. Phys.*, 1981, **72**, 2215.
66 S.-I. Chu, *J. Chem. Phys.*, 1991, **94**, 7901.
67 A. Giusti-Suzor, X. He, O. Atabek and F. H. Mies, *Phys. Rev. Lett.*, 1990, **64**, 515.
68 H. G. Muller, in *Coherence Phenomena in Atoms and Molecules in Laser Fields (NATO ASI Series B 287)*, ed. A. D. Bandrauk and S. C. Wallace, Plenum, New York, 1992, p. 89.
69 A. Giusti-Suzor, F. H. Mies, L. F. DiMauro, E. Charron and B. Yang, *J. Phys. B*, 1995, **28**, 309.
70 R. R. Freeman, P. H. Bucksbaum, H. Milchberg, S. Darack, D. Schumacher and M. E. Geusic, *Phys. Rev. Lett.*, 1987, **59**, 1092.
71 H. Helm, M. J. Der and H. Bissantz, *Phys. Rev. Lett.*, 1991, **67**, 1234.
72 G. N. Gibson, R. R. Freeman and T. J. McIlrath, *Phys. Rev. Lett.*, 1991, **67**, 1230.
73 A. Zavriyev, P. H. Bucksbaum, J. Squier and F. Saline, *Phys. Rev. Lett.*, 1993, **70**, 1077.
74 G. Yao and S.-I. Chu, *Chem. Phys. Lett.*, 1992, **197**, 413.
75 G. Yao and S.-I. Chu, *Phys. Rev. A*, 1993, **48**, 485.
76 E. E. Aubanel, A. Conjusteau and A. D. Bandrauk, *Phys. Rev. A*, 1993, **48**, R4011.
77 R. Numico, A. Keller and O. Atabek, *Phys. Rev. A*, 1997, **56**, 772.
78 G. N. Gibson, M. Li, C. Guo and J. Neira, *Phys. Rev. Lett.*, 1997, **79**, 2022.
79 L. J. Frasinski, J. H. Posthumus, J. Plumridge, K. Codling, P. F. Taday and A. J. Langley, *Phys. Rev. Lett.*, 1999, **83**, 3625.
80 L. J. Frasinski, K. Codling, P. Hatherly, J. Barr, I. N. Ross and W. T. Toner, *Phys. Rev. Lett.*, 1987, **58**, 2424.
81 K. Codling, L. J. Frasinski and P. A. Hatherly, *J. Phys. B*, 1989, **22**, L321.
82 T. Zuo and A. D. Bandrauk, *Phys. Rev. A*, 1995, **52**, 2511.
83 S. Chelkowski, T. Zuo, O. Atabek and A. D. Bandrauk, *Phys. Rev. A*, 1995, **52**, 2977.
84 J. H. Posthumus, L. J. Frasinski, A. J. Giles and K. Codling, *J. Phys. B*, 1995, **28**, L349.
85 T. Seideman, M. Yu. Ivanov and P. B. Corkum, *Phys. Rev. Lett.*, 1995, **75**, 2819.
86 M. Brewczyk, K. Rzazewski and C. W. Clark, *Phys. Rev. Lett.*, 1997, **78**, 191.
87 M. Brewczyk and K. Rzazewski, *Phys. Rev. A*, 1999, **60**, 2285.
88 Ph. Hering, M. Brewczyk and C. Cornaggia, *Phys. Rev. Lett.*, 2000, **85**, 2288.
89 M. Brewczyk and L. J. Frasinski, *J. Phys. B*, 1991, **24**, L307.
90 M. Schmidt, D. Normand and C. Cornaggia, *Phys. Rev. A*, 1994, **50**, 5037.
91 D. Normand and M. Schmidt, *Phys. Rev. A*, 1996, **53**, R1958.
92 G. N. Gibson, M. Li, C. Guo and J. P. Nibarger, *Phys. Rev. A*, 1998, **58**, 4723.
93 C. Gu, M. Li and G. N. Gibson, *Phys. Rev. Lett.*, 1999, **82**, 2492.
94 A. Iwamae, A. Hishikawa and K. Yamanouchi, *J. Phys. B*, 2000, **33**, 223.
95 A. Hishikawa, A. Iwamae and K. Yamanouchi, *Phys. Rev. Lett.*, 1999, **83**, 1127.
96 J. P. Nibarger, M. Li, S. Menon and G. N. Gibson, *Phys. Rev. Lett.*, 1999, **83**, 4975.
97 M. Nisoli, S. De Silvestri, O. Svelto, R. Szipöcs, K. Ferencz, Ch. Spielmann, S. Sartania and F. Krausz, *Opt. Lett.*, 1997, **22**, 522.
98 S. Chelkowski, P. B. Corkum and A. D. Bandrauk, *Phys. Rev. Lett.*, 1999, **82**, 3416.
99 H. Stapelfeldt, E. Constant, H. Sakai and P. B. Corkum, *Phys. Rev. A*, 1998, **58**, 426.
100 Ch. Ellert, H. Stapelfeldt, E. Constant, H. Sakai, J. Wright, D. M. Rayner and P. B. Corkum, *Philos. Trans. R. Soc. Lond. A*, 1998, **356**, 329.
101 K. C. Kulander, F. H. Mies and K. J. Schafer, *Phys. Rev. A*, 1996, **53**, 2562.
102 Ph. Hering and C. Cornaggia, *Phys. Rev. A*, 1999, **59**, 2836.
103 J. A. Fiss, L. Zhu and R. J. Gordon, *Phys. Rev. Lett.*, 1999, **82**, 65.
104 P. Lambropoulos and T. Nakajima, *Phys. Rev. Lett.*, 1999, **82**, 2266.
105 R. J. Gordon, L. Zhu and T. Seideman, *Acc. Chem. Res.*, 1999, **32**, 1007.
106 J. A. Fiss, A. Khachatrian, K. Truhins, L. Zhu, R. J. Gordon and T. Seideman, *Phys. Rev. Lett.*, 2000, **85**, 2096.
107 M. R. Thompson, M. K. Thomas, P. F. Taday, J. H. Posthumus, A. J. Langley, L. J. Frasinski and K. Codling, *J. Phys. B*, 1997, **30**, 5755.
108 Provided by the authors of, and adapted from the work in, ref. 109.
109 E. Charron, A. Giusti-Suzor and F. H. Mies, *J. Chem. Phys.*, 1995, **103**, 7359.
110 J. H. Posthumus, M. R. Thompson, A. J. Giles and K. Codling, *Phys. Rev. A*, 1996, **54**, 955.